

# Searching for EeV photons with Telescope Array Surface Detector and neural networks.

---

## Telescope Array Collaboration

R.U. Abbasi,<sup>1</sup> T. Abu-Zayyad,<sup>1,2</sup> M. Allen,<sup>2</sup> J.W. Belz,<sup>2</sup> D.R. Bergman,<sup>2</sup> F. Bradfield,<sup>3</sup> I. Buckland,<sup>2</sup> W. Campbell,<sup>2</sup> B.G. Cheon,<sup>4</sup> K. Endo,<sup>3</sup> A. Fedynitch,<sup>5,6</sup> T. Fujii,<sup>3,7</sup> K. Fujisue,<sup>5,6</sup> K. Fujita,<sup>6</sup> M. Fukushima,<sup>6</sup> G. Furlich,<sup>2</sup> A. Gálvez Ureña,<sup>8</sup> Z. Gerber,<sup>2</sup> N. Globus,<sup>9</sup> W. Hanlon,<sup>2</sup> T. Hanaoka,<sup>10</sup> N. Hayashida,<sup>11</sup> H. He,<sup>12</sup> K. Hibino,<sup>11</sup> R. Higuchi,<sup>12</sup> D. Ikeda,<sup>11</sup> D. Ivanov,<sup>2</sup> S. Jeong,<sup>13</sup> C.C.H. Jui,<sup>2</sup> K. Kadota,<sup>14</sup> F. Kakimoto,<sup>11</sup> O. Kalashev,<sup>15</sup> K. Kasahara,<sup>16</sup> Y. Kawachi,<sup>3</sup> K. Kawata,<sup>6</sup> I. Kharuk,<sup>15</sup> E. Kido,<sup>6</sup> H.B. Kim,<sup>4</sup> J.H. Kim,<sup>2</sup> J.H. Kim,<sup>2</sup> S.W. Kim,<sup>13</sup> R. Kobo,<sup>3</sup> I. Komae,<sup>3</sup> K. Komatsu,<sup>17</sup> K. Komori,<sup>10</sup> A. Korochkin,<sup>18</sup> C. Koyama,<sup>6</sup> M. Kudenko,<sup>15</sup> M. Kuroiwa,<sup>17</sup> Y. Kusumori,<sup>10</sup> M. Kuznetsov,<sup>15</sup> Y.J. Kwon,<sup>19</sup> K.H. Lee,<sup>4</sup> M.J. Lee,<sup>13</sup> B. Lubsandorzhiev,<sup>15</sup> J.P. Lundquist,<sup>20,2</sup> A. Matsuzawa,<sup>17</sup> H. Matsushita,<sup>3</sup> J.A. Matthews,<sup>2</sup> J.N. Matthews,<sup>2</sup> K. Mizuno,<sup>17</sup> M. Mori,<sup>10</sup> S. Nagataki,<sup>12</sup> K. Nakagawa,<sup>3</sup> M. Nakahara,<sup>3</sup> H. Nakamura,<sup>10</sup> T. Nakamura,<sup>21</sup> T. Nakayama,<sup>17</sup> Y. Nakayama,<sup>10</sup> K. Nakazawa,<sup>10</sup> T. Nonaka,<sup>6</sup> S. Ogio,<sup>6</sup> H. Ohoka,<sup>6</sup> N. Okazaki,<sup>6</sup> M. Onishi,<sup>6</sup> A. Oshima,<sup>22</sup> H. Oshima,<sup>6</sup> S. Ozawa,<sup>23</sup> I.H. Park,<sup>13</sup> K.Y. Park,<sup>4</sup> M. Potts,<sup>2</sup> M. Przybylak,<sup>24</sup> M.S. Pshirkov,<sup>15,25</sup> J. Remington,<sup>2</sup> C. Rott,<sup>2</sup> G.I. Rubtsov,<sup>15</sup> D. Ryu,<sup>26</sup> H. Sagawa,<sup>6</sup> N. Sakaki,<sup>6</sup> R. Sakamoto,<sup>10</sup> T. Sako,<sup>6</sup> N. Sakurai,<sup>6</sup> S. Sakurai,<sup>3</sup> D. Sato,<sup>17</sup> K. Sekino,<sup>6</sup> T. Shibata,<sup>6</sup> J. Shikita,<sup>3</sup> H. Shimodaira,<sup>6</sup> H.S. Shin,<sup>3,7</sup> K. Shinozaki,<sup>27</sup> J.D. Smith,<sup>2</sup> P. Sokolsky,<sup>2</sup> B.T. Stokes,<sup>2</sup> T.A. Stroman,<sup>2</sup> H. Tachibana,<sup>3</sup> K. Takahashi,<sup>6</sup> M. Takeda,<sup>6</sup> R. Takeishi,<sup>6</sup> A. Taketa,<sup>28</sup> M. Takita,<sup>6</sup> Y. Tameda,<sup>10</sup> K. Tanaka,<sup>29</sup> M. Tanaka,<sup>30</sup> M. Teramoto,<sup>10</sup> S.B. Thomas,<sup>2</sup> G.B. Thomson,<sup>2</sup> P. Tinyakov,<sup>18,15</sup> I. Tkachev,<sup>15</sup> T. Tomida,<sup>17</sup> S. Troitsky,<sup>15</sup> Y. Tsunesada,<sup>3,7</sup> S. Udo,<sup>11</sup> F.R. Urban,<sup>8</sup> M. Vrábel,<sup>27</sup> D. Warren,<sup>12</sup> K. Yamazaki,<sup>22</sup> Y. Zhezher,<sup>6,15</sup> Z. Zundel,<sup>2</sup> J. Zvirzdin,<sup>2</sup>

<sup>1</sup>Department of Physics, Loyola University-Chicago, Chicago, Illinois 60660, USA

<sup>2</sup>High Energy Astrophysics Institute and Department of Physics and Astronomy, University of Utah, Salt Lake City, Utah 84112-0830, USA

<sup>3</sup>Graduate School of Science, Osaka Metropolitan University, Sugimoto, Sumiyoshi, Osaka 558-8585, Japan

<sup>4</sup>Department of Physics and The Research Institute of Natural Science, Hanyang University, Seongdong-gu, Seoul 426-791, Korea

<sup>5</sup>Institute of Physics, Academia Sinica, Taipei City 115201, Taiwan

<sup>6</sup>Institute for Cosmic Ray Research, University of Tokyo, Kashiwa, Chiba 277-8582, Japan

<sup>7</sup>Nambu Yoichiro Institute of Theoretical and Experimental Physics, Osaka Metropolitan University, Sugimoto, Sumiyoshi, Osaka 558-8585, Japan

<sup>8</sup>CEICO, Institute of Physics, Czech Academy of Sciences, Prague 182 21, Czech Republic

<sup>9</sup>Institute of Astronomy, National Autonomous University of Mexico Ensenada Campus, Ensenada, BC 22860, Mexico

<sup>10</sup>Graduate School of Engineering, Osaka Electro-Communication University, Neyagawa-shi, Osaka 572-8530, Japan

<sup>11</sup>Faculty of Engineering, Kanagawa University, Yokohama, Kanagawa 221-8686, Japan

- <sup>12</sup>*Astrophysical Big Bang Laboratory, RIKEN, Wako, Saitama 351-0198, Japan*
- <sup>13</sup>*Department of Physics, Sungkyunkwan University, Jang-an-gu, Suwon 16419, Korea*
- <sup>14</sup>*Department of Physics, Tokyo City University, Setagaya-ku, Tokyo 158-8557, Japan*
- <sup>15</sup>*Institute for Nuclear Research of the Russian Academy of Sciences, Moscow 117312, Russia*
- <sup>16</sup>*Faculty of Systems Engineering and Science, Shibaura Institute of Technology, Minumaku, Tokyo 337-8570, Japan*
- <sup>17</sup>*Academic Assembly School of Science and Technology Institute of Engineering, Shinshu University, Nagano, Nagano 380-8554, Japan*
- <sup>18</sup>*Service de Physique Théorique, Université Libre de Bruxelles, Brussels 1050, Belgium*
- <sup>19</sup>*Department of Physics, Yonsei University, Seodaemun-gu, Seoul 120-749, Korea*
- <sup>20</sup>*Center for Astrophysics and Cosmology, University of Nova Gorica, Nova Gorica 5297, Slovenia*
- <sup>21</sup>*Faculty of Science, Kochi University, Kochi, Kochi 780-8520, Japan*
- <sup>22</sup>*College of Science and Engineering, Chubu University, Kasugai, Aichi 487-8501, Japan*
- <sup>23</sup>*Quantum ICT Advanced Development Center, National Institute for Information and Communications Technology, Koganei, Tokyo 184-8795, Japan*
- <sup>24</sup>*Doctoral School of Exact and Natural Sciences, University of Lodz, Lodz, Lodz 90-237, Poland*
- <sup>25</sup>*Sternberg Astronomical Institute, Moscow M.V. Lomonosov State University, Moscow 119991, Russia*
- <sup>26</sup>*Department of Physics, School of Natural Sciences, Ulsan National Institute of Science and Technology, UNIST-gil, Ulsan 689-798, Korea*
- <sup>27</sup>*Astrophysics Division, National Centre for Nuclear Research, Warsaw 02-093, Poland*
- <sup>28</sup>*Earthquake Research Institute, University of Tokyo, Bunkyo-ku, Tokyo 277-8582, Japan*
- <sup>29</sup>*Graduate School of Information Sciences, Hiroshima City University, Hiroshima, Hiroshima 731-3194, Japan*
- <sup>30</sup>*Institute of Particle and Nuclear Studies, KEK, Tsukuba, Ibaraki 305-0801, Japan*

*E-mail:* [ivan.kharuk@phystech.edu](mailto:ivan.kharuk@phystech.edu)

**ABSTRACT:** Ultra-high-energy photons play an important role in probing astrophysical models and beyond-Standard-Model scenarios. We report updated limits on the diffuse photon flux using Telescope Array’s Surface Detector data collected over 14 years of operation. Our method employs a neural network classifier to effectively distinguish between proton-induced and photon-induced events. The input data include both reconstructed composition-sensitive parameters and raw time-resolved signals registered by the Surface Detector stations. To mitigate biases from Monte Carlo simulations, we fine-tune the network with a subset of experimental data. The number of observed photon candidates is found to be consistent with the expected hadronic background, yielding upper limits on photon flux  $\Phi_\gamma(E_\gamma > 10^{19}\text{eV}) < 2.3 \cdot 10^{-3}$ , and  $\Phi_\gamma(E_\gamma > 10^{20}\text{eV}) < 3.0 \cdot 10^{-4} (\text{km}^2 \cdot \text{sr} \cdot \text{yr})^{-1}$ .

---

## Contents

<b>1</b>	<b>Introduction</b>	<b>1</b>
<b>2</b>	<b>Method</b>	<b>2</b>
<b>3</b>	<b>Data sets and Monte Carlo simulations</b>	<b>4</b>
<b>4</b>	<b>Neural network</b>	<b>6</b>
4.1	Architecture	6
4.2	Training Process	9
<b>5</b>	<b>Model dependence</b>	<b>10</b>
<b>6</b>	<b>Results</b>	<b>10</b>
<b>7</b>	<b>Conclusions</b>	<b>14</b>
<b>A</b>	<b>Reconstruction procedure</b>	<b>15</b>
<b>B</b>	<b>Results without fine-tuning</b>	<b>16</b>

---

## 1 Introduction

Ultra-high-energy (UHE) photons of astrophysical origin, with energies above  $10^{18}$  eV, are of interest for two main reasons. First, they can be produced via the Greisen-Zatsepin-Kuzmin (GZK) mechanism [1–7] in the interstellar medium. The resulting photon flux depends on the mass composition of cosmic rays, thus providing an independent tool for their analyses. Second, registering ultra-high-energy photons beyond the expected GZK flux level would provide strong evidence for models beyond the Standard Model of particle physics [8–10], including, in particular, decaying dark matter [11–17] and violation of Lorentz symmetry [18–21].

Experimental searches for ultra-high-energy photons rely on complementary detection techniques, each with distinct advantages and limitations. Fluorescence Detectors measure fluorescence light from extensive air showers (EAS), allowing for the direct observation of the longitudinal shower development and the depth of shower maximum ( $X_{max}$ ). This provides excellent discrimination between photon and hadron primaries, but their operation time is restricted to clear, moonless nights, resulting in a limited duty cycle that constrains the exposure accumulation for ultra-high-energy events. Conversely, scintillator-based Surface Detectors, measuring secondary particles at the ground level, operate continuously, offering the vast exposure required to probe low-flux regimes. However, they face challenges in distinguishing muon and electromagnetic components of EAS, whose ratio is the key for distinguishing hadron-induced and photon-induced EAS. To address this,

experiments like Yakutsk [22] employed dedicated muon detectors to suppress the hadronic background. Similarly, the Pierre Auger Observatory has set stringent limits in the Southern Hemisphere by utilizing both hybrid observations [23] and water-Cherenkov Surface Detectors [24], which possess different sensitivities to the muon component compared to scintillators. Early constraints were also established by the AGASA experiment [25]. None of the experiments reported an excess of photon-induced events above the expected hadronic background, producing photon-like events due to fluctuations of EAS evolution.

In this paper, we search for ultra-high-energy photons using Telescope Array (TA) experiment data. TA is a large-scale cosmic ray experiment located in Utah, USA,  $39^{\circ}17'49''$  N  $112^{\circ}54'31''$  W, at approximately 1.4 km above sea level [26–28]. It aims to study ultra-high-energy cosmic rays (UHECR) using its Surface Detector (SD), Fluorescence Detector (FD), and Low Energy (TALE) extension. Operating since 2008, TA has accumulated a large number of EAS events, allowing for thorough studies of cosmic ray properties.

Unlike FD, SD operates under almost all weather conditions, but provides less informative data. To compensate for this, we employ a neural network classifier that is capable of leveraging complex patterns in data to effectively discern between photon- and proton-induced events. In the astrophysical field, neural networks have been successfully applied in TA [29–31], Pierre Auger Observatory [32–34], KASCADE-Grande [35], and neutrino telescopes [36–41]. These examples illustrate the potential of using machine learning in our analysis using TA SD data.

Our method incorporates a blind optimization of the neural network classification threshold to establish the most stringent constraint on the photon flux. To mitigate discrepancies between Monte Carlo simulations and the experimental data, the technique includes a procedure for fine-tuning the neural networks using a relevant subset of the experimental data. This allows us to achieve robust and efficient separation between hadron-induced and photon-induced EAS.

The TA SD array, depicted in Figure 1, comprises 507 above-ground scintillation stations arranged in a square grid covering an area of approximately  $700 \text{ km}^2$ . Each SD station consists of two layers of plastic scintillator, which register signals with a time resolution of 20 ns [26]. All stations are calibrated in real time using atmospheric muons, with the signal measured in conventional units called a "minimal ionizing particles" (MIPs). For our analysis, we retain 128 consecutive time bins from each layer of triggered SD stations, which we refer to as waveforms. An example of a waveform registered by a single SD station is presented in Figure 2.

The sensitivity threshold of the TA SD for photon-induced events is approximately  $10^{18.1} \text{ eV}$  (see Figure 3). While this allows us to derive an integral limit for  $E > 10^{18} \text{ eV}$ , the very limited exposure between  $10^{18}$  and  $10^{18.5} \text{ eV}$  implies that such a limit would be dominated almost entirely by higher-energy photons, and hence could be misleading. We therefore present results only for  $E > 10^{18.5} \text{ eV}$ , where the TA SD has sufficient direct sensitivity.

## 2 Method

We start by outlining the general scheme of the analysis and stating our main assumptions. The method comprises four main steps, which we describe below.

1. *Data selection and preparation.* We perform Monte Carlo (MC) simulations of 14 years of TA SD data, modeling air showers initiated by protons and photons. Heavy nuclei such as iron

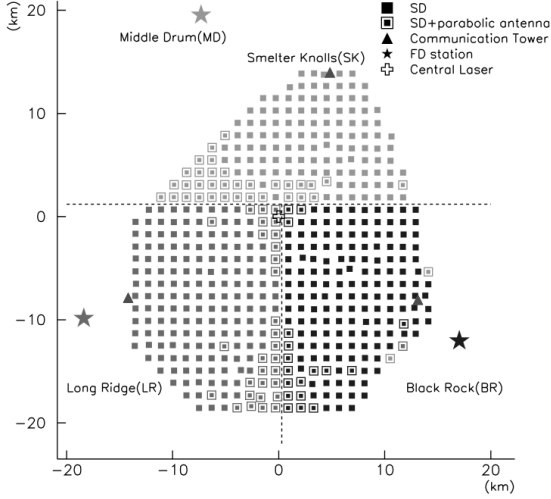


**Figure 1.** Schematic representation of the arrangement of the TA SD and FD stations, [26].

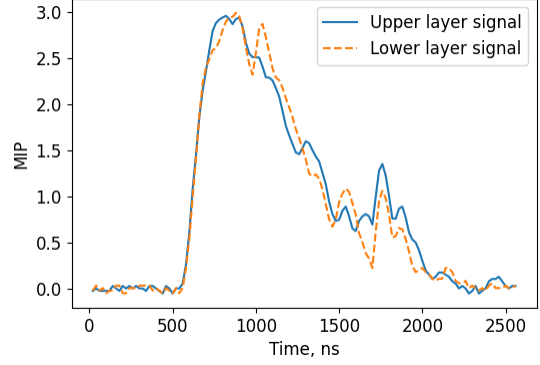


**Figure 2.** An example of processed and calibrated waveforms registered by a TA SD station. Blue and orange lines depict signals from the upper and lower scintillator layers, respectively.

produce showers that develop earlier, exhibit denser cores, and higher muon-to-electromagnetic ratios than proton-induced cascades [42–44]. This makes them easier to distinguish from photon-induced air showers, yielding protons as the main background source to photons signal.

2. *Neural network training.* We train a neural network classifier to distinguish between proton- and photon-induced EAS events using a MC-simulated data set. For each event the neural network outputs a number  $\xi \in [0; 1]$  representing its confidence that a given event is proton-like (closer to 0) or photon-like (closer to 1).

Monte Carlo simulations might have slight differences from experimental data that are irrelevant for standard algorithmic reconstruction but are utilized by the neural network. To account for this fact, we fine-tune the neural network using a subset of the experimental data confidently identified as proton-induced events (see Section 4.2 for details). This step allows the neural network to learn from actual data, thus reducing MC-specific biases. The data used at this step is not used in the subsequent computation of the photon flux upper limit. In what follows, we refer to this set as the burn sample.

3. *Blind optimization of the classification threshold.* At present, the most energetic photons observed in the experiment have energies of the order of PeV [45, 46]. Strong constraints have been set on the upper limit of photon flux at EeV energies [24, 47–51] without detecting photon signal — the number of observed photon candidates was consistent with background expectations. Based on this, we optimize the neural network’s classification threshold to provide the strongest constraint on the photon flux after unblinding the data and calculating the actual number of photon candidates.

For a given classification threshold  $\xi$ , the 95% upper limit on photon flux  $\Phi$  can be calculated as the ratio of 95% confidence level on the number of observed photon candidates,  $\sigma^{95}(n^{\text{cand}}(\xi))$ , to the effective TA SD exposure,  $\Omega(\xi)$ :

$$\Phi_{\gamma} = \frac{\sigma^{95}(n^{\text{cand}}(\xi))}{\Omega(\xi)} . \quad (2.1)$$

We minimize this value by performing blind optimization of the classification threshold on the MC

data set assuming HiRes [52] and  $E^{-2}$  differential energy spectra for proton and photon primaries, respectively.

The effective TA SD exposure is the product of the following factors: data collection time; product of area and solid angle used in the MC simulation; trigger efficiency (ratio of events that invoked TA SD trigger to the total number of MC events); event selection efficiency (fraction of events passing quality cuts after the reconstruction); and photons selection efficiency,  $S(\xi) = \frac{n_\gamma(\xi)}{n_\gamma(0)}$ , where  $n_\gamma(\xi)$  is the number of photons passing neural network's classification threshold. Note that only photon selection efficiency depends on  $\xi$ . Hence all other factors can be omitted for the classification threshold optimization.

The estimation of the numerator in Equation 2.1 requires a multi-step procedure. Initially, the proton suppression level,  $P(\xi)$ , is quantified on the MC sample. It is defined as the ratio of events incorrectly identified as photons to the total number of proton events for a given  $\xi$ . Subsequently, the expected number of false photons due to the proton background in the experimental data,  $n^{\text{bg}}(\xi)$ , is estimated by multiplying  $P(\xi)$  by the total number of experimental events. Further, the corresponding 95% confidence level upper limit is determined using the Feldman-Cousins statistics [53] under the assumption of zero background, which is designated as  $\sigma^{95}(n^{\text{bg}}(\xi))$ . Given that event registration is inherently a random process,  $n^{\text{bg}}(\xi)$  should be considered as a Poisson random variable, hence optimizing  $\sigma^{95}(n^{\text{bg}}(\xi))$  expectation value.

Putting all together, we fix  $\xi_{\text{opt}}$  on MC proton and photon data sets by minimizing

$$L^{95} = \frac{M(\sigma^{95}(n^{\text{bg}}(\xi)))}{S(\xi)}, \quad (2.2)$$

where  $M(\cdot)$  stands for the expectation value.

4. *Obtaining photon flux limits.* As the final step of the analysis, we unblind the data and count the number of photons candidates that passed the classification threshold optimized in the previous step. This gives  $n^{\text{cand}}(\xi_{\text{opt}})$ , substituting which into Eq. 2.1 yields the resulting limit on the diffuse photon flux.

In the following sections, we describe in detail the data and Monte Carlo sets along with the neural network architecture and training. The final results are presented in Section 6.

### 3 Data sets and Monte Carlo simulations

In this study we use TA SD data recorded during 14 years of observation between 2008-05-11 and 2022-05-10. We process the data and MC simulations using the same reconstruction procedure and apply the same event quality cuts, as described below.

MC simulations conducted for this study encompass the complete evolution of air showers and the subsequent response of TA SD stations. These simulations are performed to model 14 years of TA operation, using CORSIKA [54] for air shower simulations and GEANT4 [55] for detector response modeling. The simulations adhered to the actual real-time calibration tables of the TA SD to ensure an accurate representation of the detector behavior.

For proton-induced events, we employed three high-energy hadronic interaction models: QGSJET-II-04 [56], EPOS-LHC [57], and Sibyll 2.3d [58]. Low-energy hadronic and electromagnetic interactions were simulated using FLUKA [59] and EGS4 [60], correspondingly.

The simulations were performed in three energy ranges, starting from  $10^{17.45}$ ,  $10^{18.95}$ , and  $10^{19.45}$  eV. Within each sample, the proton energy spectrum is modeled to follow the one measured by the HiRes experiment [52]. Due to the sharp drop-off of the spectrum at high energies, such splitting is required for a comprehensive comparison of the MC and experimental data at different energy scales. These datasets were subsequently used for setting upper limits on photon flux at different energy cutoffs. The number of simulated air showers is the same for all of the high-energy hadronic interaction models.

Photon-induced events are simulated using the QGSJET-II-04, FLUKA, and EGS4. We use the PRESHOWER code [61] to account for geomagnetic interactions resulting in magnetic  $e^+$ ,  $e^-$  pair production. The corresponding air showers are dominated by their electromagnetic component, hence the effect of choosing a particular high-energy hadron interaction model should be negligible. We test this assumption with Monte Carlo simulations in Section 5. The differential energy spectrum is chosen to be  $E^{-1}$  to cover the whole range of energies within a single data set, thus avoiding underrepresentation of high-energy events.

MC and experimental data were passed through a reconstruction procedure [62] optimized to infer the parameters of photon-induced events. We estimate the energy of events based on the look-up table constructed using MC photon data set [51], which is a function of the reconstructed  $S_{800}$  value (scintillator signal density at the distance of 800 m from the core), zenith and azimuth angles. Thus obtained energy corresponds to average energy of the primary photon, inducing a shower with the same arrival direction and  $S_{800}$ . The full list of reconstructed features, presented in Appendix A, includes geometrical and primary particle mass-sensitive parameters, such as reconstructed zenith angle and Linsley front curvature.

To ensure good quality of events reconstruction, we applied the following selection criteria to both the MC and the experimental data sets:

- Reconstructed zenith angle is below  $55^\circ$ ;
- Minimum of 7 triggered stations per event;
- Reconstructed shower core position is within the SD array, at least 1200 meters from its boundary;
- Joint geometry and lateral distribution profile fit accuracy of  $\chi^2/d.o.f. < 5$ .

The chosen set of event quality cuts is closer to the standard ones used for anisotropy studies with proton primaries in TA. It provides a balance between reconstruction accuracy and photon exposure. Note that the cut in the zenith angle is slightly stricter than in our previous studies [51, 63]. Additionally, since it is impossible to properly simulate the signal in the saturated stations, we exclude them both from MC-simulated and experimental data.

To create a balanced data set for neural network training and evaluation, we employ a mixing procedure for proton-induced and photon-induced events. The energy range is divided into bins of constant width (0.05 in  $\log_{10}$  scale), in each of which the events are randomly sampled so that the total number of registered and successfully reconstructed events of both types is equal. This makes the energy spectrum of proton- and photon-induced events the same, which mitigates potential biases related to event energy, which could otherwise be exploited by the neural network as a discriminative yet unphysical parameter. The resulting energy spectrum of events passing event quality cuts in MC sample is presented in Figure 3.

The final MC sample comprises approximately  $5 \cdot 10^6$  events in total, which is mixture of



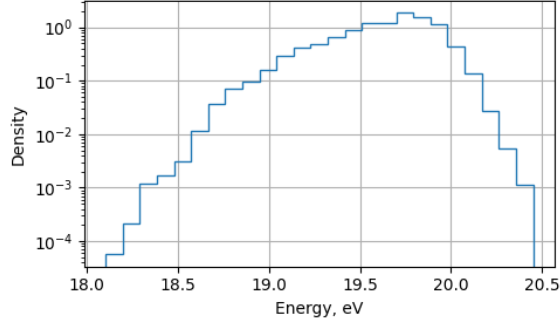


**Figure 3.** Energy distribution of the MC sample used for neural network training with mixed photon-induced and proton-induced events after applying event selection criteria.

proton primaries for all three hadronic interaction models and photon primaries. Events were partitioned into training, test, and validation sets in a ratio of 8:1:1. The test data set is utilized for optimizing neural network parameters, while the validation data set serves for blind optimization of the classification threshold and estimation of TA SD exposure.

For the experimental data, we have excluded all lightning-correlated events. That is, we reject events registered within a 10-minute interval related to lightnings recorded by the National Lightning Detection Network [64] at the location of the TA SD. This step is necessary as lightning can be registered by TA SD as photon-like events [65].

## 4 Neural network

### 4.1 Architecture

The neural network architecture used in this study is a slight modification of the one used previously for the analysis of mass composition [66] and the estimation of the flux of photons [67]. Its architecture, presented in Figure 4, consists of three main components, each focusing on different aspects of the cosmic ray-induced air shower:

(1) *Spatial station bundle.* This component analyses the geometric pattern of activated SD stations. It treats each event as an “image” on a 6x6 grid of stations centered around the reconstructed shower core. This representation allows the network to identify the spatial features of an air shower. Convolutional neural networks are known to be well suited for analyzing such data, allowing for efficient parsing of the geometrical structure of an event.

For each of the stations on the grid, the input data includes:

- Stations coordinates relative to the reconstructed position of the shower core;
- Integral charge registered by the station;
- Reconstructed time of the shower plane front arrival;
- Time difference between the actual station activation time and the plane front arrival;
- Mask whether the station was triggered in an event or not.

The splitting of station activation time into two components, items 4 and 5 in the list above, is useful as it provides the neural network the information on the front curvature. The data for the stations that were not triggered in an event are filled with zeros.



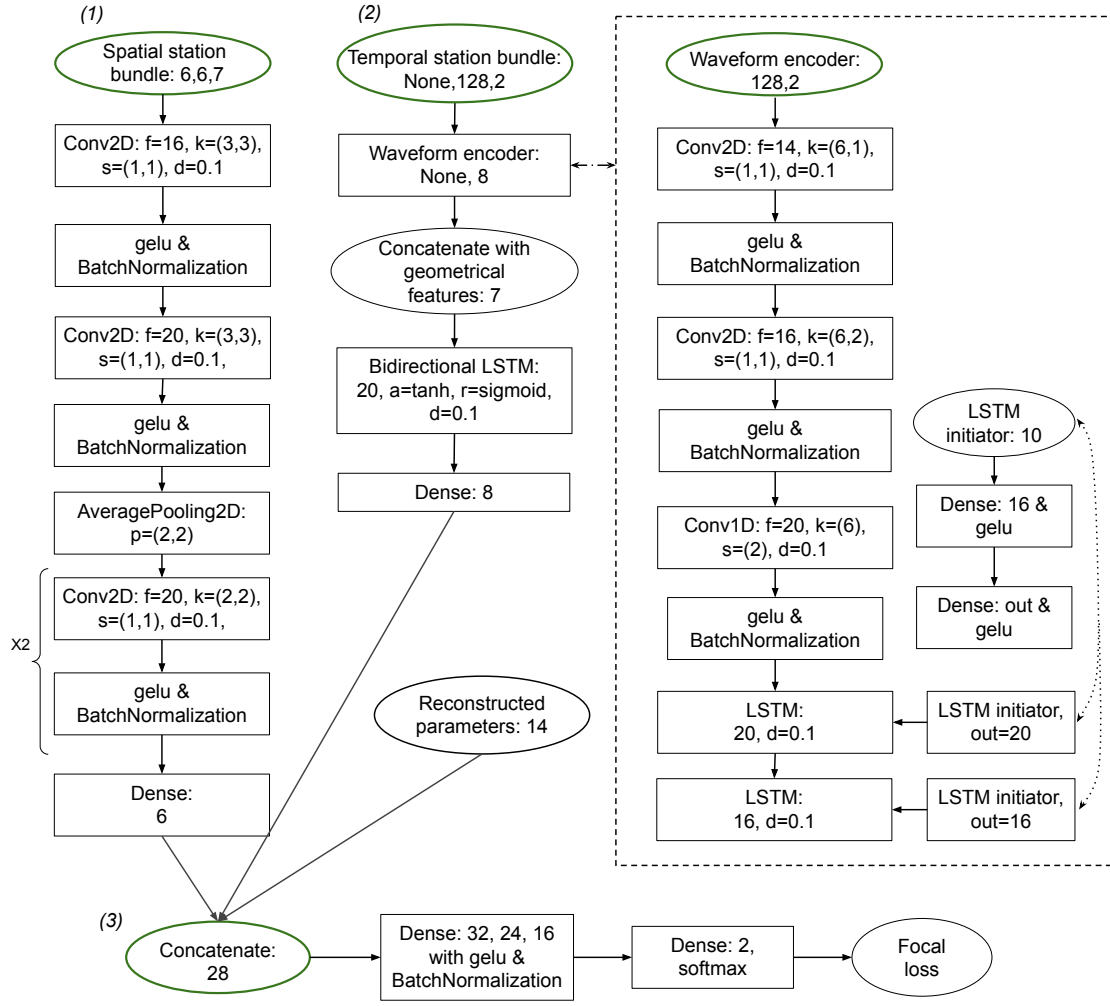


**Figure 4.** Architecture of the neural network used to distinguish proton-induced and photon-induced events: (1) – spatial station bundle, (2) – temporal station bundle, and (3) – combined analysis. The waveform encoder architecture, which is a sub-network in the temporal station bundle, is shown inside the dotted box. Solid arrows depict data flow, dotted lines connect elements with their detailed description. Layer names and parameters follow TensorFlow API.

(2) *Temporal station bundle.* The triggered stations naturally form a time series when ordered according to their activation times. This sequence captures the structure of an air shower, specifically how it evolves from the periphery to the center and again to the periphery, thus providing the neural network with useful information. The diagram of data processing in this part of the neural network is depicted in Figure 5 and goes as follows:

- (i) The input data comprises a set of SD stations ordered according to their activation times (red dashed boxes in Figure 5). Unlike the spatial station bundle, in this part of the neural network we also use raw waveforms registered by the stations.
- (ii) First, waveforms of all SD station are passed through a *waveform encoder*, which extracts features representing waveform characteristics using a combination of convolutional and

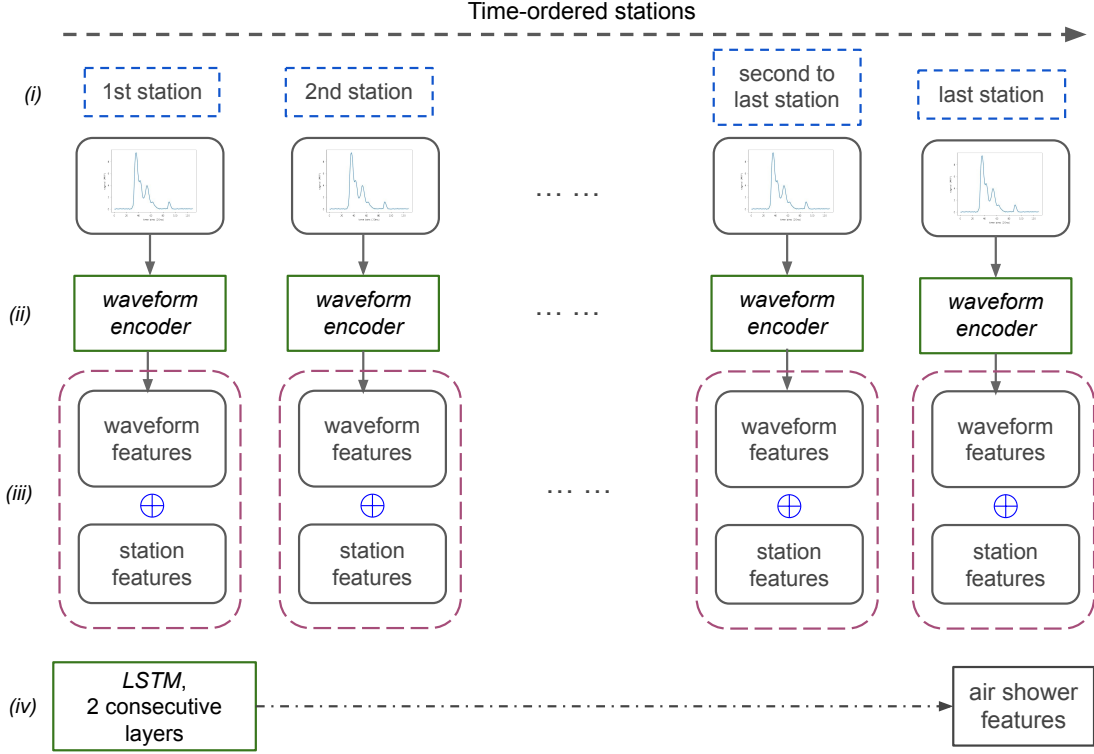


**Figure 5.** Architecture of the temporal station bundle. See the temporal station bundle in Figure 4 for layers characteristics.

recurrent layers. In particular, we use *LSTM initiator* sub-network to initialize the state of the recurrent layers, utilizing reconstructed event properties, station coordinates and activation times (see Fig. 4).

- (iii) Second, thus extracted features are concatenated with individual station features – their coordinates, activation times, and integral registered charges. This yields full set of station features, represented as magenta dashed boxes in Figure 5.
- (iv) Finally, the resulting “station sequence” is passed through a bidirectional Long Short-Term Memory layer, which outputs event characteristics as a whole.

(3) *Combined analysis.* To infer whether an event was proton- or photon-induced, we concatenate the features extracted by the *spatial station bundle* and the *temporal station bundle*. We supplement this data with reconstructed event characteristics, such as primary zenith and azimuth angles,  $S_{800}$ , and others (see Appendix A). Together, they are passed through a series of fully connected (dense) layers. The output of the last layer is a number  $\xi \in [0; 1]$  representing the neural network’s confidence that the corresponding event is photon-like.

In total, the neural network has 29000 trainable parameters. We used the Adam optimizer [68] and employ early stopping for terminating neural network training. The neural network is implemented using the TensorFlow library [69].

We explored the importance of each of the neural network components described above by training a neural network with only one of them. The temporal station bundle, reconstruction

parameters, and spatial station bundle yielded 96%, 85%, and 81% separation accuracy, respectively. We would like to note that it was essential to combine all of these blocks in a single architecture to achieve the best metrics.

## 4.2 Training Process

To optimize the neural network capability for separating proton- and photon-induced events, we employed several training techniques:

(1) **Weighted training.** We assigned higher weights to proton-induced events during training (specifically, five for protons and one for photons). The choice of class weights is a hyperparameter optimized to enhance the final sensitivity of the analysis. Since our goal is to set the strongest constraints on the photon flux, the optimal estimator should minimize the false-positive rate (proton background misidentified as photons) in the critical signal region ( $\xi \approx 1$ ), even at the cost of overall classification balance. This strategic prioritization of proton rejection is a deliberate feature of the training optimization. It does not bias the final flux estimation, as the validity of the classifier's performance is ensured by the agreement between its predictions on MC-simulated and experimental data.

(2) We used a special loss function, namely, *focal loss* [70]:

$$L = (1 - p_c)^\gamma \ln p_c, \quad (4.1)$$

where  $p_c$  is the neural networks confidence for the correct class and  $\gamma$  is a constant, which we fixed to be two. The term  $(1 - p_c)^\gamma$  modulates the standard cross-entropy loss so that events that were assigned to the correct class with high confidence yield small contribution to the total loss value. Hence neural network pays more attention to events that are difficult to classify.

(3) **Ensemble approach.** We trained multiple neural networks and selected the top three based on their metrics for constraining the photon flux, Eq. 2.2. This approach helps mitigate biases that may arise from the sensitivity of individual networks to specific event features.

Monte Carlo simulations inevitably involve simplifications, such as the application of thinning and de-thinning procedures [71], as well as uncertainties related to the modeling of air shower evolution and the response of detector stations. To account for such imperfections, and avoid overfitting to MC data as opposed to experimental data, we employed two complementary strategies.

First, for neural network training we introduced physically motivated noise into the simulated data, mimicking the resolution of the input parameters. This includes both additive Gaussian noise (40 ns for station activation times and 0.1 MIP for waveform signals) and multiplicative noise for measured charge (10%).

Second, a fine-tuning procedure based on a burn sample of experimental data was implemented. After the initial training of the neural network on MC simulations, the model was used to evaluate the photon-likeness of experimental events. Events that were classified with high confidence ( $\xi \leq 0.2$ ) as proton-induced were included in the training set with corresponding labels. The network was then fine-tuned on this augmented data set, where each training batch contained equal fractions of simulated and experimental proton-induced events. Training was terminated after the burn sample was passed twice through the network, a choice made to prevent overfitting to the limited experimental subset.

Using a burn sample to fine-tune the neural network constitutes the novelty of our approach. It helps the network adapt to the nuances of real data that may not be fully captured in simulations. Importantly, we observed that the effect of using burn sample on neural network metrics is negligible, indicating that there are no major MC-experimental data discrepancies. This step was inspired by surrogate supervision and labeling [72], where a limited subset of data with approximate or indirectly obtained annotations is employed to guide model adaptation to new domains.

## 5 Model dependence

Before analyzing the experimental data, we investigated the dependence of neural network predictions on the choice of high-energy hadronic interaction model. To this end, we trained two neural networks: one using events simulated with QGSJET-II-04 and EPOS-LHC as high-energy hadronic interaction models and the other using all available models (including Sibyll). For this study, we did not perform fine-tuning of neural networks on experimental data.

Figure 6 presents histograms of neural network predictions for proton-induced events in the common test data set. We use two samples, starting from  $10^{17.45}$  eV and  $10^{18.95}$  eV, to separately study high-energy events. For the MC  $10^{17.45}$  eV and  $10^{18.95}$  eV samples, the predictions of neural networks are similar for all hadronic interaction models for both neural networks. The sole notable exception is that EPOS-LHC produces more photon-like events in the rightmost bin for the  $10^{18.95}$  eV sample. For the MC  $10^{19.45}$  eV sample, the events simulated with Sibyll are more photon-like, up to a factor of two in each bin. This discrepancy is less pronounced, yet significant, for the neural network trained on all hadronic interaction models.

We also examined the model dependence of neural network predictions for photon-induced air showers. Figure 7 illustrates the histograms of the neural network predictions for Monte Carlo events simulated using QGSJET-II-04 and EPOS-LHC. The histograms exhibit a discrepancy for proton-like events ( $\xi < 0.1$ ) but are in good agreement for  $\xi > 0.5$ . This observation shows that the evolution of photon-induced air showers exhibits some dependence on the choice of hadronic interaction model. However, for non-proton-like events ( $\xi > 0.5$ ), which are of primary interest for this study, the difference is negligible. This justifies our decision to use only one hadronic interaction model for simulating photon-induced air showers.

Based on these observations, we conclude that at energies below  $10^{19.5}$  eV the effect of choosing a particular hadronic interaction model is negligible. At higher energies the effect becomes more pronounced.

Given that no single hadronic interaction model is inherently preferable, we opted to train neural networks using all available hadronic interaction models. This approach serves to mitigate the model dependence of the predictions and thus provides a robust upper limit on photon flux.

## 6 Results

Now we present the results of applying the analysis described above to the TA SD data collected during 14 years of observation.

Figure 8 depicts histograms of neural network predictions for MC and experimental data across various energy thresholds. The predictions for proton MC and experimental data demonstrate good

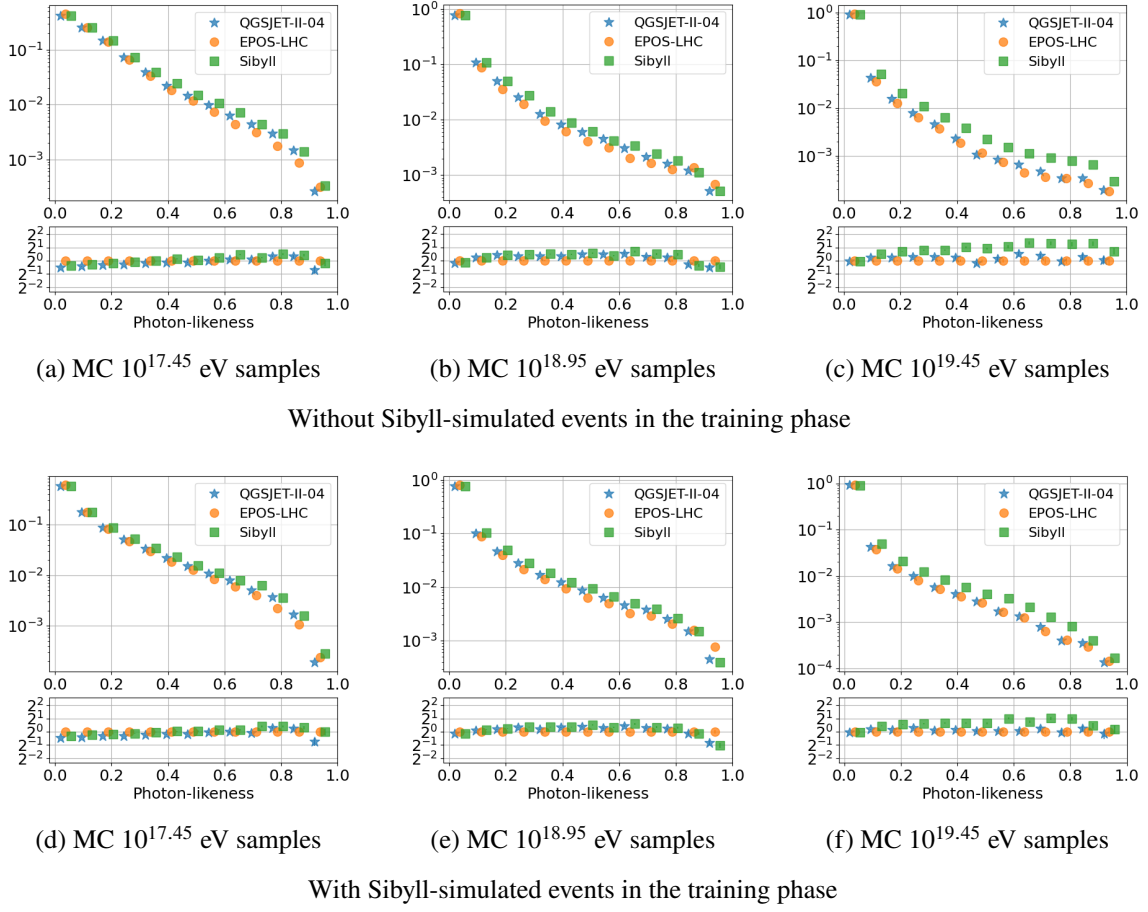


**Figure 6.** Comparison of the histograms of neural network predictions on proton-induced MC samples simulated using different high-energy hadronic interaction models. The vertical axis shows the number of events in the corresponding bin. The lower subplots depict the ratios of events in the histogram bins with respect to events simulated using EPOS-LHC. To avoid overlapping, points for different hadronic interaction models are slightly shifted horizontally.

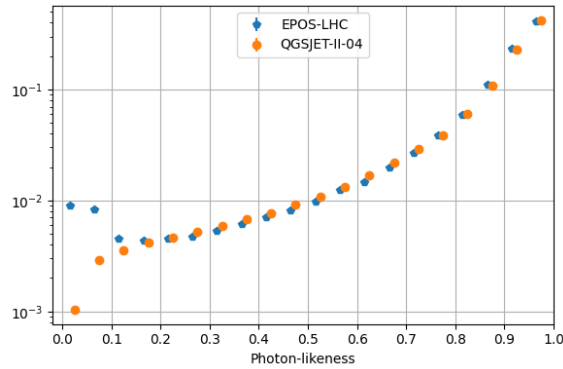


**Figure 7.** Comparison of neural network predictions for photon-induced air showers simulated using QGSJET-II-04 and EPOS-LHC hadronic interaction models.

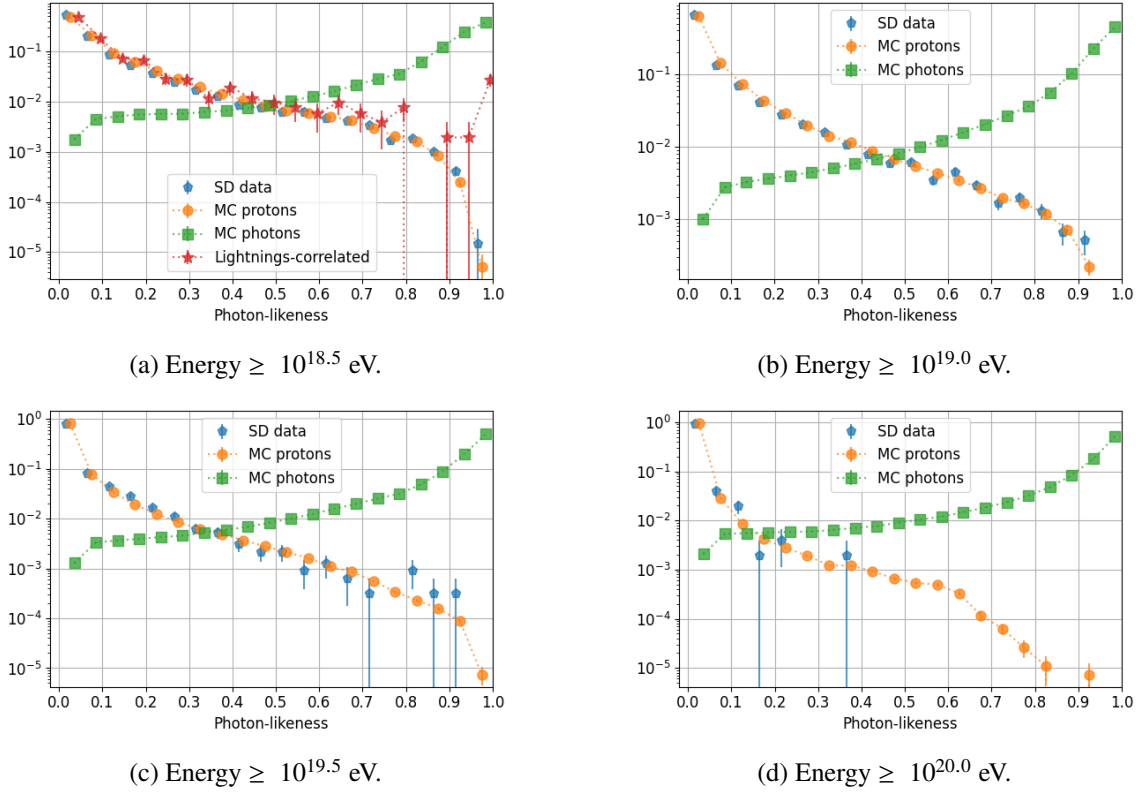


**Figure 8.** Histograms of neural network predictions for SD and MC data at various energy cuts. Error bars denote statistical uncertainties.

agreement. Importantly, there is no evidence of overfitting to the SD data in the region  $\xi \in [0, 0.2]$ , which was used to fine-tune the neural network.

The same distributions, obtained without fine-tuning the neural networks on experimental data, are shown in Figure 10 in Appendix B. The fine-tuning procedure significantly improved the agreement between proton MC and experimental data. This improvement is quantified by the mean asymmetric ratio between the histogram bins, which was reduced from 5.1 to 1.2 for events with  $E > 10^{18.5}$  eV.

As an additional validation measure, we examined the neural network’s predictions on events correlated with lightning strikes registered near TA SD, Figure 8a. The corresponding histogram exhibits a peak near  $\xi = 1$ , indicating that some of the events are indeed lightning-induced. We have also identified Terrestrial Gamma-Ray Flashes and lightning-correlated events previously reported by TA as photon-like with high confidence [73–75]. This confirms that the neural network correctly learned to identify photon-like events since lightning-induced events are essentially electromagnetic cascades, which are similar to photon-induced air showers [73].

To derive upper limits on the photon flux, we use Eq. 2.1. We calculate the effective TA SD exposure taking into account TA SD geometry, event selection and trigger efficiency, exclusion of events below the classification threshold, and the use of burn sample for fine-tuning the neural network. The efficiency of quality and  $\xi$  cuts along with the effective exposure is shown in Table 1.

The resulting limits on photon flux are presented in Table 2. We observed no significant excess

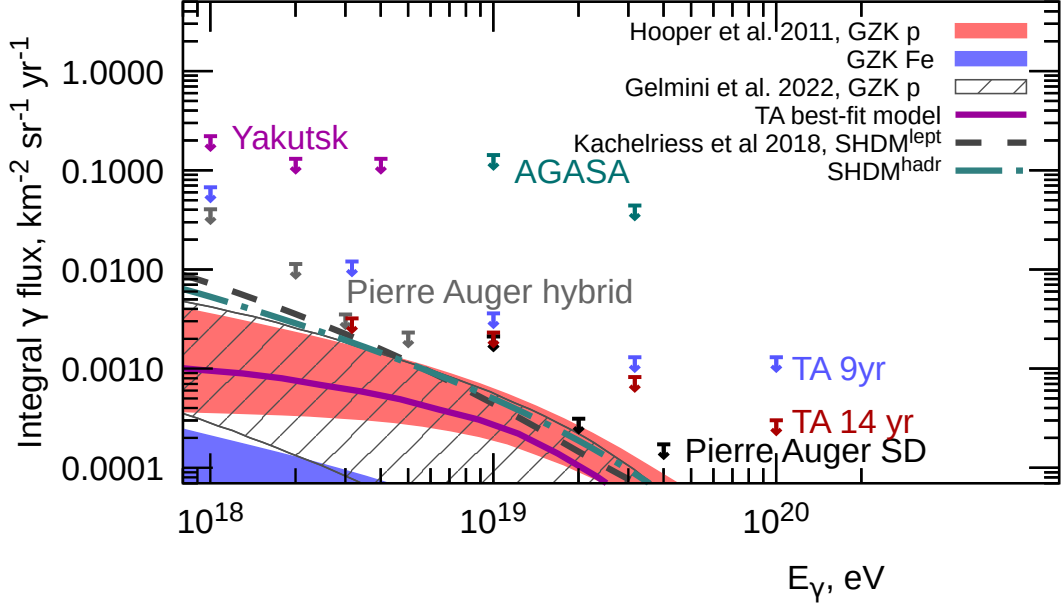


**Figure 9.** Upper limits on diffuse flux of UHE photons obtained in this study (TA 14 yr) compared with the previous TA result [51] and limits obtained by AGASA [25], Yakutsk [22], and Pierre Auger hybrid [23] and SD [24]. For comparison we show the expected flux of cosmogenic UHE photons for several UHECR flux models: pure protons (red band [6] and hatched band [7]), pure iron (blue band [6]), in both cases the bands denote the theoretical uncertainties of the models, and TA best-fit model [76, 77]. The predictions for SHDM decaying via hadronic and leptonic channels are also shown [78].

Energy, $\log_{10}(E/1\text{eV})$	Quality cuts	$\xi$ -cut	$\xi$ -cut value	Effective exposure, $10^3 \text{ km}^2 \cdot \text{sr} \cdot \text{yr}$
18.5	22.8%	25.4%	0.95	0.98
19.0	46.1%	45.9%	0.932	3.58
19.5	58.2%	64.2%	0.909	6.30
20.0	67.7%	91.4%	0.691	10.44

**Table 1.** Contributions of the cuts to the effective exposure at each energy threshold. The value represents the ratio of the exposure after the given cut to the exposure before cut. The value of the optimal  $\xi$ -cut is given for reference.

of photon candidates compared to the expected proton background. The upper limits on the photon fraction were calculated as a ratio of the corresponding photon flux limit to the integral flux of the TA SD spectrum [79]. In Fig. 9 we compare the present limits with the limits of AGASA [25], Yakutsk [22] and Pierre Auger hybrid [23] and SD observations [24]. For comparison we depict the previous TA limits obtained using boosted decision trees for 9 years of SD operation time [51]. In the same figure we also show theoretical predictions for the UHE photon flux. The predictions for cosmogenic photons (GZK photons) depend on the mass composition of initial UHECR flux:



Energy, $\log_{10}(E/\text{eV})$	Effective exposure, $10^3 \text{ km}^2 \cdot \text{sr} \cdot \text{yr}$	Proton suppres- sion level	Expected photon candidates (from proton bg.)	Observed photon candidates	Photon flux upper limit, $(\text{km}^2 \cdot \text{sr} \cdot \text{yr})^{-1}$	Photon fraction upper limit
18.5	0.98	$8.2 \cdot 10^{-6}$	0.35	0	$3.2 \cdot 10^{-3}$	$1.3 \cdot 10^{-3}$
19.0	3.58	$4.4 \cdot 10^{-5}$	0.62	3	$2.3 \cdot 10^{-3}$	$6.8 \cdot 10^{-3}$
19.5	6.30	$5.6 \cdot 10^{-5}$	0.18	1	$8.2 \cdot 10^{-4}$	$2.1 \cdot 10^{-2}$
20.0	10.44	$1.2 \cdot 10^{-4}$	0.06	0	$3.0 \cdot 10^{-4}$	0.21

**Table 2.** Resulting metrics and limits on the photon flux. Effective exposure is evaluated after imposing both the event quality cuts and the  $\xi$  cut.

pure protons [6, 7] and pure iron nuclei [6] are shown as extreme cases. The uncertainties of the predicted photon fluxes due to uncertainties of the initial UHECR flux and its propagation are shown as bands. We also show the prediction of the cosmogenic UHE photon flux [77] for the UHECR flux model derived as a best fit for the TA spectrum and  $X_{\text{max}}$  data [76]. The expectations for UHE photon fluxes from the decay of super heavy dark matter (SHDM) particles  $X$  are shown for two benchmark models:  $X \rightarrow q\bar{q}$  and  $X \rightarrow \nu\bar{\nu}$  [78]. In both cases the  $X$  mass,  $M_X$ , is  $10^{12}$  eV and the its lifetime,  $\tau_X$ , is normalized to the Pierre Auger hybrid limits [23], which are the most stringent constraints for these scenarios. Specifically, we use  $\tau_X = 7.1 \times 10^{22}$  yr for the  $X \rightarrow q\bar{q}$  model and  $\tau_X = 1.7 \times 10^{22}$  yr for the  $X \rightarrow \nu\bar{\nu}$  model.

## 7 Conclusions

In this work, we have presented an updated search for the diffuse flux of ultra-high-energy photons using a 14-year data set from the Telescope Array Surface Detector. By employing a neural network classifier that combines reconstructed composition-sensitive observables with time-resolved SD waveforms, and fine-tuning it with a dedicated burn sample of experimental data, we achieved a robust and efficient separation between photon-induced and proton-induced events. Together with the increased statistics of the TA SD data set, this leads to a substantial improvement over our previous results, in particular at the energy thresholds of  $10^{18.5}$  and  $10^{20.0}$  eV, where the constraints are strengthened by approximately a factor of three. At intermediate energies, the sensitivity improvement is moderated by the observation of a small number of photon candidates, which remain consistent with statistical fluctuations of the expected hadronic background. As a result, we derived stringent 95% confidence level upper limits on the photon flux, which are the most strict in the Northern Hemisphere and complement the limits set by the Pierre Auger Observatory in the Southern Hemisphere.

We found no significant excess of photon candidates above the expected hadronic background. Our limits approach the upper edge of the GZK photon predictions [6, 7]; however, probing the GZK photon models [77] will require an improvement of several times in sensitivity. Notably, in the search for signals from SHDM decay, our limits are competitive with those of Auger, despite

the fact that TA does not observe the Galactic center region, which is abundant for the dark matter. Looking ahead, we hope to support or constrain such models in future with increased TA SD exposure time or improved machine learning-based event selection criteria.

## Code Availability

Code for reproducing the architecture of the neural network described in section 4 is available at <https://github.com/ml-inr/TA-gamma-search>.

## Acknowledgments

The Telescope Array experiment is supported by the Japan Society for the Promotion of Science(JSPS) through Grants-in-Aid for Priority Area 431, for Specially Promoted Research JP21000002, for Scientific Research (S) JP19104006, for Specially Promoted Research JP15H05693, for Scientific Research (S) JP19H05607, for Scientific Research (S) JP15H05741, for Science Research (A) JP18H03705, for Young Scientists (A) JPH26707011, for Transformative Research Areas (A) JP25H01294, for International Collaborative Research 24KK0064, and for Fostering Joint International Research (B) JP19KK0074, by the joint research program of the Institute for Cosmic Ray Research (ICRR), The University of Tokyo; by the Pioneering Program of RIKEN for the Evolution of Matter in the Universe (r-EMU); by the U.S. National Science Foundation awards PHY-1806797, PHY-2012934, PHY-2112904, PHY-2209583, PHY-2209584, and PHY-2310163, as well as AGS-1613260, AGS-1844306, and AGS-2112709; by the National Research Foundation of Korea (2017K1A4A3015188, 2020R1A2C1008230, and RS-2025-00556637) ; by the Ministry of Science and Higher Education of the Russian Federation under the contract 075-15-2024-541, IISN project No. 4.4501.18, by the Belgian Science Policy under IUAP VII/37 (ULB), by National Science Centre in Poland grant 2020/37/B/ST9/01821, by the European Union and Czech Ministry of Education, Youth and Sports through the FORTE project No. CZ.02.01.01/00/22\_008/0004632, and by the Simons Foundation (MP-SCMPS-00001470, NG). This work was partially supported by the grants of the joint research program of the Institute for Space-Earth Environmental Research, Nagoya University and Inter-University Research Program of the Institute for Cosmic Ray Research of University of Tokyo. The foundations of Dr. Ezekiel R. and Edna Wattis Dumke, Willard L. Eccles, and George S. and Dolores Doré Eccles all helped with generous donations. The State of Utah supported the project through its Economic Development Board, and the University of Utah through the Office of the Vice President for Research. The experimental site became available through the cooperation of the Utah School and Institutional Trust Lands Administration (SITLA), U.S. Bureau of Land Management (BLM), and the U.S. Air Force. We appreciate the assistance of the State of Utah and Fillmore offices of the BLM in crafting the Plan of Development for the site. We thank Patrick A. Shea who assisted the collaboration with much valuable advice and provided support for the collaboration's efforts. The people and the officials of Millard County, Utah have been a source of steadfast and warm support for our work which we greatly appreciate. We are indebted to the Millard County Road Department for their efforts to maintain and clear the roads which get us to our sites. We gratefully acknowledge the contribution from the technical staffs of our home institutions. An allocation of computing resources from the Center for High Performance Computing at the University of Utah as well as the Academia Sinica Grid Computing Center (ASGC) is gratefully acknowledged. The lightning data used in this paper was obtained from Vaisala, Inc. We appreciate Vaisala's academic research policy.

## A Reconstruction procedure

The reconstruction procedure employs a joint fit of the event geometry and lateral distribution function [62]. The fit incorporates seven free parameters:

- 1-2) Position of the shower core,  $\vec{r}_{\text{core}} = (x_{\text{core}}, y_{\text{core}}, 0)$ ;
- 3-4) Arrival direction of the primary particle: zenith ( $\theta$ ) and azimuth ( $\phi$ ) angles;
- 5) Normalization of the shower's lateral distribution profile,  $S_{800}$ ;
- 6) Time offset,  $t_0$ ;
- 7) Linsley front curvature parameter,  $a$ .

The fit optimizes two target functions: the SD stations activation times  $t(\vec{r})$  and their deposited charges  $S(r)$ ,

$$t(\vec{r}) = t_0 + t_{\text{plane}}(\vec{r}) + a \times LDF(r)^{-0.5} \times \left(1 + \frac{r}{R_l}\right)^{1.5}, \quad (\text{A.1a})$$

$$S(r) = S_{800} \times LDF(r), \quad (\text{A.1b})$$

where  $r$  is the distance from the station to the shower core (i.e. the shortest distance between a point and a line),  $t_{\text{plane}}(\vec{r})$  is the arrival time of the shower's plane front to the station located at  $\vec{r}$ , and  $LDF(r)$  is the empirical lateral distribution profile introduced in the AGASA experiment [80] and fine-tuned to better fit TA data [81]:

$$t_{\text{plane}}(\vec{r}) = \frac{1}{c} \times (\vec{n}, (\vec{r} - \vec{r}_{\text{core}})), \quad (\text{A.2a})$$

$$LDF(r) = f(r)/f(r_0), \quad r_0 = 800 \text{ m}, \quad (\text{A.2b})$$

$$f(r) = \left(\frac{r}{R_m}\right)^{-1.2} \left(1 + \frac{r}{R_m}\right)^{-(\eta-1.2)} \left(1 + \frac{r^2}{R_l^2}\right)^{-0.6}. \quad (\text{A.2c})$$

Here  $c$  is the speed of light,  $\vec{n} = \vec{n}(\theta, \phi)$  is the unit vector along the direction of the shower axis,  $(\cdot, \cdot)$  stands for the scalar product, and

$$R_m = 90 \text{ m}, \quad R_l = 1000 \text{ m}, \quad R_l = 30 \text{ m}, \quad (\text{A.3a})$$

$$\eta = 3.97 - 1.79(\sec(\theta) - 1). \quad (\text{A.3b})$$

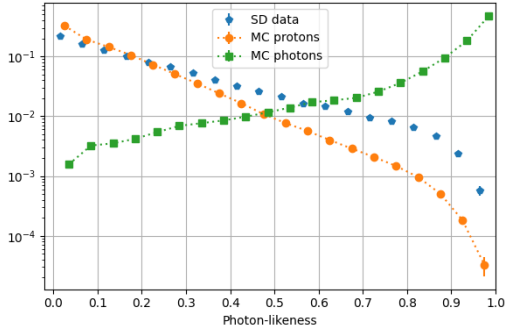
The energy of the primary particle is estimated as a function of  $S_{800}$ ,  $\theta$ , and  $\phi$  using a lookup table obtained from the photon MC simulations [51].

Below is the list of 14 reconstructed parameters [51] used as input data for the neural network:

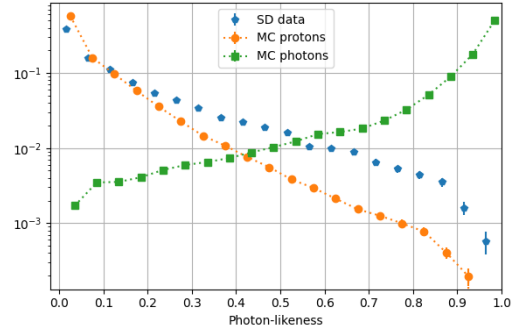
- 1) Reconstructed Linsley front curvature parameter ( $a$ );
- 2-3) Zenith and azimuth angles ( $\theta$ ,  $\phi$ );
- 4) Signal density at 800 m from the shower core ( $S_{800}$ );
- 5)  $\chi^2/d.o.f.$  for the joint geometry and LDF fit;
- 6-7) Area-over-peak of the signal at 1200 m and the corresponding slope parameter [82];
- 8-9)  $S_b \equiv \sum_i \left(S_i \times \left(\frac{r_i}{r_0}\right)^b\right)$  for two values of  $b$ : 2.5 and 4.0. Here  $S_i$  and  $r_i$  are the integral signal of  $i$ -th station and its distance to the shower core, respectively, and  $r_0 = 1200 \text{ m}$  [42];
- 10) Sum of integral signals from all of the triggered stations.
- 11) Asymmetry of the signal between the upper and lower layers of stations [83];
- 12) Total number of peaks within all stations [83];
- 13) Number of peaks for the station with the largest signal;
- 14) Minimal distance between the reconstructed air shower core and SD array edge.

## B Results without fine-tuning

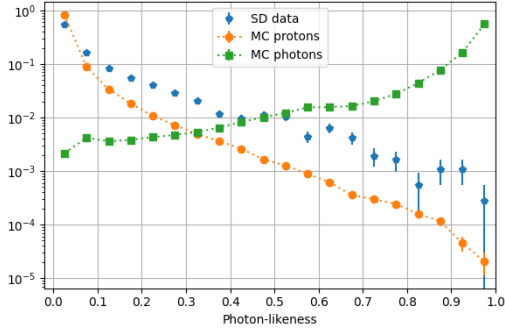
Figure 10 presents histograms of neural network predictions on experimental and MC simulated data without the fine-tuning process described in the main text. In this case, SD events exhibit more photon-like



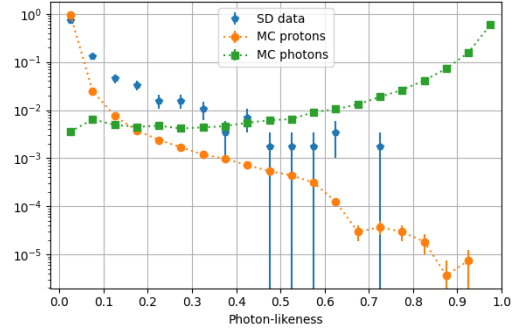
(a) Energy  $\geq 10^{18.5}$  eV.



(b) Energy  $\geq 10^{19.0}$  eV.



(c) Energy  $\geq 10^{19.5}$  eV.



(d) Energy  $\geq 10^{20.0}$  eV.

**Figure 10.** Histograms of neural network prediction for SD and MC data at various energy cuts without fine-tuning using experimental data. Error bars denote statistical uncertainty.

characteristics than MC data. This discrepancy can be due to small differences between MC and experimental data that are irrelevant for the standard reconstruction, but are important for the neural network. Fine-tuning the neural network on SD data mitigates these differences, resulting in more reliable predictions.

Our analysis revealed that the weighting scheme applied to proton- and photon-induced events during neural network training influences the consistency of MC and experimental data histograms. Specifically, assigning higher weights to photon events tends to increase the similarity between these histograms. However, we retain our original weighting ratio for two reasons. Firstly, this weighting strategy compels the neural network to minimize false-positive photon identifications, which is crucial for setting stronger limits on photon flux. Secondly and more importantly, altering the weights based on observed outcomes would compromise the blind nature of our analysis.

## References

- [1] K. Greisen, *End to the cosmic-ray spectrum?*, *Physical Review Letters* **16** (1966) 748.
- [2] G. T. Zatsepin and V. A. Kuzmin, *Upper limit of the spectrum of cosmic rays*, *JETP Lett.* **4** (1966) 78–80.
- [3] J. Wdowczyk, W. Tkaczyk, C. Adcock and A. W. Wolfendale, *The possibility of detectable fluxes of cosmic ray gamma rays with energy above 10-to-the-19 ev*, *J. Phys. A* **4** (1971) L37–L39.
- [4] W. Michalak, J. Wdowczyk and A. W. Wolfendale, *Cosmic gamma-rays and neutrinos of energy near 10<sup>20</sup> eV*, *J. Phys. G* **16** (1990) 1917–1924.

- [5] G. B. Gelmini, O. E. Kalashev and D. V. Semikoz, *GZK Photons Above 10-EeV*, *JCAP* **11** (2007) 002, [[0706.2181](#)].
- [6] D. Hooper, A. M. Taylor and S. Sarkar, *Cosmogenic photons as a test of ultra-high energy cosmic ray composition*, *Astropart. Phys.* **34** (2011) 340–343, [[1007.1306](#)].
- [7] G. B. Gelmini, O. Kalashev and D. Semikoz, *Upper Limit on the Diffuse Radio Background from GZK Photon Observation*, *Universe* **8** (2022) 402, [[2206.00408](#)].
- [8] V. Berezhinsky, P. Blasi and A. Vilenkin, *Signatures of topological defects*, *Physical Review D* **58** (1998) 103515.
- [9] L. A. Anchordoqui et al., *Hunting super-heavy dark matter with ultra-high energy photons*, *Astropart. Phys.* **132** (2021) 102614, [[2105.12895](#)].
- [10] M. Fairbairn, T. Rashba and S. V. Troitsky, *Photon-axion mixing and ultra-high-energy cosmic rays from BL Lac type objects - Shining light through the Universe*, *Phys. Rev. D* **84** (2011) 125019, [[0901.4085](#)].
- [11] V. Berezhinsky, M. Kachelriess and A. Vilenkin, *Ultrahigh-energy cosmic rays without GZK cutoff*, *Phys. Rev. Lett.* **79** (1997) 4302–4305, [[astro-ph/9708217](#)].
- [12] V. A. Kuzmin and V. A. Rubakov, *Ultrahigh-energy cosmic rays: A Window to postinflationary reheating epoch of the universe?*, *Phys. Atom. Nucl.* **61** (1998) 1028, [[astro-ph/9709187](#)].
- [13] V. A. Kuzmin and I. I. Tkachev, *Ultrahigh-energy cosmic rays and inflation relics*, *Phys. Rept.* **320** (1999) 199–221, [[hep-ph/9903542](#)].
- [14] O. K. Kalashev and M. Y. Kuznetsov, *Constraining heavy decaying dark matter with the high energy gamma-ray limits*, *Phys. Rev. D* **94** (2016) 063535, [[1606.07354](#)].
- [15] O. Kalashev, M. Kuznetsov and Y. Zhezher, *Constraining superheavy decaying dark matter with directional ultra-high energy gamma-ray limits*, *JCAP* **11** (2021) 016, [[2005.04085](#)].
- [16] M. Chianese, D. F. G. Fiorillo, R. Hajjar, G. Miele and N. Saviano, *Constraints on heavy decaying dark matter with current gamma-ray measurements*, *JCAP* **11** (2021) 035, [[2108.01678](#)].
- [17] S. Das, K. Murase and T. Fujii, *Revisiting ultrahigh-energy constraints on decaying superheavy dark matter*, *Phys. Rev. D* **107** (2023) 103013, [[2302.02993](#)].
- [18] S. Coleman and S. L. Glashow, *High-energy tests of lorentz invariance*, *Physical Review D* **59** (1999) 116008.
- [19] M. Galaverni and G. Sigl, *Lorentz violation for photons and ultrahigh-energy cosmic rays*, *Physical review letters* **100** (2008) 021102.
- [20] G. Rubtsov, P. Satunin and S. Sibiryakov, *Prospective constraints on lorentz violation from ultrahigh-energy photon detection*, *Physical Review D* **89** (2014) 123011.
- [21] PIERRE AUGER collaboration, P. Abreu et al., *Testing effects of Lorentz invariance violation in the propagation of astroparticles with the Pierre Auger Observatory*, *JCAP* **01** (2022) 023, [[2112.06773](#)].
- [22] A. V. Glushkov, I. T. Makarov, M. I. Pravdin, I. E. Slepsov, D. S. Gorbunov, G. I. Rubtsov et al., *Constraints on the flux of primary cosmic-ray photons at energies  $E > 10^{18}$  eV from Yakutsk muon data*, *Phys. Rev. D* **82** (2010) 041101, [[0907.0374](#)].
- [23] PIERRE AUGER collaboration, A. Abdul Halim et al., *Search for photons above  $10^{18}$  eV by simultaneously measuring the atmospheric depth and the muon content of air showers at the Pierre Auger Observatory*, *Phys. Rev. D* **110** (2024) 062005, [[2406.07439](#)].

- [24] P. Abreu, M. Aglietta, I. Allekotte, K. A. Cheminant, A. Almela, J. Alvarez-Muñiz et al., *Search for photons above  $10^{19}$  eV with the surface detector of the Pierre Auger Observatory*, *Journal of Cosmology and Astroparticle Physics* **2023** (2023) 021.
- [25] K. Shinozaki et al., *Upper limit on gamma-ray flux above  $10^{19}$ -eV estimated by the Akeno Giant Air Shower Array experiment*, *Astrophys. J. Lett.* **571** (2002) L117–L120.
- [26] T. Abu-Zayyad, R. Aida, M. Allen, R. Anderson, R. Azuma, E. Barcikowski et al., *The surface detector array of the telescope array experiment*, *Nuclear Instruments and Methods in Physics Research Section A: Accelerators, Spectrometers, Detectors and Associated Equipment* **689** (2012) 87–97.
- [27] H. Tokuno, Y. Tameda, M. Takeda, K. Kadota, D. Ikeda, M. Chikawa et al., *New air fluorescence detectors employed in the telescope array experiment*, *Nuclear Instruments and Methods in Physics Research Section A: Accelerators, Spectrometers, Detectors and Associated Equipment* **676** (2012) 54–65.
- [28] S. Udo, S. Ogioa, M. Takeda, T. Nonaka, H. Sagawa, Y. Tsunesada et al., *The telescope array low-energy extension*, in *35th International Cosmic Ray Conference (ICRC2017)*, vol. 301, p. 544, 2017.
- [29] TELESCOPE ARRAY collaboration, O. Kalashev, *Using Deep Learning in Ultra-High Energy Cosmic Ray Experiments*, *J. Phys. Conf. Ser.* **1525** (2020) 012001.
- [30] D. Ivanov, O. E. Kalashev, M. Y. Kuznetsov, G. I. Rubtsov, T. Sako, Y. Tsunesada et al., *Using deep learning to enhance event geometry reconstruction for the telescope array surface detector*, *Mach. Learn. Sci. Tech.* **2** (2021) 015006, [2005.07117].
- [31] O. Kalashev, I. Kharuk, M. Kuznetsov, G. Rubtsov, T. Sako, Y. Tsunesada et al., *Deep learning method for identifying mass composition of ultra-high-energy cosmic rays*, *JINST* **17** (2022) P05008, [2112.02072].
- [32] PIERRE AUGER collaboration, A. Aab et al., *Deep-learning based reconstruction of the shower maximum  $X_{max}$  using the water-Cherenkov detectors of the Pierre Auger Observatory*, *JINST* **16** (2021) P07019, [2101.02946].
- [33] PIERRE AUGER collaboration, A. Abdul Halim et al., *Mass Composition from 3 EeV to 100 EeV using the Depth of the Maximum of Air-Shower Profiles Estimated with Deep Learning using Surface Detector Data of the Pierre Auger Observatory*, *PoS ICRC2023* (2023) 278.
- [34] PIERRE AUGER collaboration, J. Glombitza, *Air-Shower Reconstruction at the Pierre Auger Observatory based on Deep Learning*, *PoS ICRC2019* (2020) 270.
- [35] M. Y. Kuznetsov, N. A. Petrov, I. A. Plokhikh and V. V. Sotnikov, *Energy spectra of elemental groups of cosmic rays with the KASCADE experiment data and machine learning*, *JCAP* **05** (2024) 125, [2312.08279].
- [36] ICECUBE collaboration, M. Huennefeld, *Deep Learning in Physics exemplified by the Reconstruction of Muon-Neutrino Events in IceCube*, *PoS ICRC2017* (2018) 1057.
- [37] ICECUBE collaboration, M. Huennefeld et al., *Combining Maximum-Likelihood with Deep Learning for Event Reconstruction in IceCube*, *PoS ICRC2021* (2021) 1065, [2107.12110].
- [38] KM3NeT collaboration, C. De Sio, *Machine Learning in KM3NeT*, *EPJ Web Conf.* **207** (2019) 05004.
- [39] KM3NeT collaboration, B. Spisso, *Event Analysis in KM3NeT Using Machine Learning*, *ASP Conf. Ser.* **532** (2022) 195.



- [40] I. Kharuk, G. Rubtsov and G. Safronov, *Rejecting noise in Baikal-GVD data with neural networks*, [\*JINST\* \*\*18\*\* \(2023\) P09026](#), [[2210.04653](#)].
- [41] I. Kharuk, G. Safronov, A. Matseiko and A. Leonov, *Machine learning in Baikal-GVD experiment*, [\*PoS ICRC2023\* \(2023\) 1077](#).
- [42] G. Ros, A. D. Supanitsky, G. A. Medina-Tanco, L. del Peral, J. C. D’Olivo, M. D. Rodriguez-Frias et al., *A new composition-sensitive parameter for Ultra-High Energy Cosmic Rays*, [\*Astropart. Phys.\* \*\*35\*\* \(2011\) 140–151](#), [[1104.3399](#)].
- [43] G. Ros, A. D. Supanitsky, G. Medina-Tanco, L. Del Peral and M. Rodriguez-Frias, *Improving photon-hadron discrimination based on cosmic ray surface detector data*, *Astroparticle Physics* **47** (2013) 10–17.
- [44] L. Cazon, R. Conceição and F. Riehn, *Universality of the muon component of extensive air showers*, *Journal of Cosmology and Astroparticle Physics* **2023** (2023) 022.
- [45] TIBET ASGAMMA collaboration, M. Amenomori et al., *First Detection of sub-PeV Diffuse Gamma Rays from the Galactic Disk: Evidence for Ubiquitous Galactic Cosmic Rays beyond PeV Energies*, [\*Phys. Rev. Lett.\* \*\*126\*\* \(2021\) 141101](#), [[2104.05181](#)].
- [46] LHAASO collaboration, Z. Cao et al., *Ultrahigh-energy photons up to 1.4 petaelectronvolts from 12  $\gamma$ -ray Galactic sources*, [\*Nature\* \*\*594\*\* \(2021\) 33–36](#).
- [47] Y. A. Fomin, N. N. Kalmykov, I. S. Karpikov, G. V. Kulikov, M. Y. Kuznetsov, G. I. Rubtsov et al., *Constraints on the flux of  $\sim (10^{16} - 10^{17.5})$  eV cosmic photons from the EAS-MSU muon data*, [\*Phys. Rev. D\* \*\*95\*\* \(2017\) 123011](#), [[1702.08024](#)].
- [48] KASCADE GRANDE collaboration, W. D. Apel et al., *KASCADE-Grande Limits on the Isotropic Diffuse Gamma-Ray Flux between 100 TeV and 1 EeV*, [\*Astrophys. J.\* \*\*848\*\* \(2017\) 1](#), [[1710.02889](#)].
- [49] PIERRE AUGER collaboration, A. Abdul Halim et al., *Search for a diffuse flux of photons with energies above tens of PeV at the Pierre Auger Observatory*, [2502.02381](#).
- [50] A. Aab, P. Abreu, M. Aglietta, I. Al Samarai, I. Albuquerque, I. Allekotte et al., *Search for photons with energies above  $10^{18}$  eV using the hybrid detector of the pierre auger observatory*, *Journal of Cosmology and Astroparticle Physics* **2017** (2017) 009.
- [51] TELESCOPE ARRAY collaboration, R. U. Abbasi et al., *Constraints on the diffuse photon flux with energies above  $10^{18}$  eV using the surface detector of the Telescope Array experiment*, [\*Astropart. Phys.\* \*\*110\*\* \(2019\) 8–14](#), [[1811.03920](#)].
- [52] HiRES collaboration, R. U. Abbasi et al., *First observation of the Greisen-Zatsepin-Kuzmin suppression*, [\*Phys. Rev. Lett.\* \*\*100\*\* \(2008\) 101101](#), [[astro-ph/0703099](#)].
- [53] G. J. Feldman and R. D. Cousins, *A Unified approach to the classical statistical analysis of small signals*, [\*Phys. Rev. D\* \*\*57\*\* \(1998\) 3873–3889](#), [[physics/9711021](#)].
- [54] D. Heck, J. Knapp, J. N. Capdevielle, G. Schatz and T. Thouw, *CORSIKA: A Monte Carlo code to simulate extensive air showers*, .
- [55] GEANT4 collaboration, S. Agostinelli et al., *GEANT4—a simulation toolkit*, [\*Nucl. Instrum. Meth. A\* \*\*506\*\* \(2003\) 250–303](#).
- [56] S. Ostapchenko, *QGSJET-II: towards reliable description of very high energy hadronic interactions*, *Nuclear Physics B-Proceedings Supplements* **151** (2006) 143–146.
- [57] T. Pierog and K. Werner, *Epos model and ultra high energy cosmic rays*, *Nuclear Physics B-Proceedings Supplements* **196** (2009) 102–105.



- [58] E.-J. Ahn, R. Engel, T. K. Gaisser, P. Lipari and T. Stanev, *Cosmic ray interaction event generator sibyll 2.1*, *Physical Review D* **80** (2009) 094003.
- [59] A. Ferrari, J. Ranft, P. R. Sala and A. Fassò, *FLUKA: A multi-particle transport code (Program version 2005)*. No. CERN-2005-10. Cern, 2005.
- [60] W. R. Nelson, H. Hirayama and D. W. Rogers, *Egs4 code system*, tech. rep., Stanford Linear Accelerator Center, Menlo Park, CA (USA), 1985.
- [61] P. Homola, D. Gora, D. Heck, H. Klages, J. Pekala, M. Risse et al., *Simulation of ultrahigh energy photon propagation in the geomagnetic field*, *Comput. Phys. Commun.* **173** (2005) 71–90, [[astro-ph/0311442](#)].
- [62] TELESCOPE ARRAY collaboration, T. Abu-Zayyad et al., *Upper limit on the flux of photons with energies above  $10^{19}$  eV using the Telescope Array surface detector*, *Phys. Rev. D* **88** (2013) 112005, [[1304.5614](#)].
- [63] TELESCOPE ARRAY collaboration, R. U. Abbasi et al., *Search for point sources of ultra-high-energy photons with the Telescope Array surface detector*, *Mon. Not. Roy. Astron. Soc.* **492** (2020) 3984–3993, [[1904.00300](#)].
- [64] K. L. Cummins and M. J. Murphy, *An overview of lightning locating systems: History, techniques, and data uses, with an in-depth look at the us nldn*, *IEEE transactions on electromagnetic compatibility* **51** (2009) 499–518.
- [65] R. Abbasi, M. Abe, T. Abu-Zayyad, M. Allen, R. Anderson, R. Azuma et al., *The bursts of high energy events observed by the telescope array surface detector*, *Physics Letters A* **381** (2017) 2565–2572.
- [66] O. Kalashev, I. Kharuk, M. Kuznetsov, G. Rubtsov, T. Sako, Y. Tsunesada et al., *Deep learning method for identifying mass composition of ultra-high-energy cosmic rays*, *Journal of Instrumentation* **17** (2022) P05008.
- [67] TELESCOPE ARRAY collaboration, I. Kharuk, G. Rubtsov and M. Kuznetsov, *Search for EeV photon-induced events at the Telescope Array*, *PoS ICRC2023* (2023) 324.
- [68] D. P. Kingma and J. Ba, *Adam: A method for stochastic optimization*, *arXiv preprint arXiv:1412.6980* (2014) .
- [69] M. Abadi, A. Agarwal, P. Barham, E. Brevdo, Z. Chen, C. Citro et al., *TensorFlow: Large-scale machine learning on heterogeneous systems*, 2015.
- [70] T.-Y. Lin, P. Goyal, R. Girshick, K. He and P. Dollár, *Focal loss for dense object detection*, in *Proceedings of the IEEE international conference on computer vision*, pp. 2980–2988, 2017.
- [71] B. T. Stokes, R. Cady and D. Ivanov, *Using CORSIKA to quantify Telescope Array surface detector response*, in *32nd International Cosmic Ray Conference*, vol. 2, p. 254, 2011, [DOI](#).
- [72] N. Tajbakhsh, Y. Hu, J. Cao, X. Yan, Y. Xiao, Y. Lu et al., *Surrogate supervision for medical image analysis: Effective deep learning from limited quantities of labeled data*, in *2019 IEEE 16th International Symposium on Biomedical Imaging (ISBI 2019)*, pp. 1251–1255, 2019, [DOI](#).
- [73] N. Kieu, R. Abbasi, M. M. F. Saba, J. Belz, P. Krehbiel, M. A. Stanley et al., *First time-resolved leader spectra associated with a downward terrestrial gamma-ray flash detected at the telescope array surface detector*, *Journal of Geophysical Research: Atmospheres* **129** (2024) e2024JD041720.
- [74] R. U. Abbasi et al., *Intermediate Fluence Downward Terrestrial Gamma Ray Flashes as Observed by the Telescope Array Surface Detector*, *J. Geophys. Res. Atmos.* **129** (2024) e2024JD041260.

- [75] TELESCOPE ARRAY PROJECT collaboration, R. U. Abbasi et al., *The bursts of high energy events observed by the telescope array surface detector*, *Phys. Lett. A* **381** (2017) 2565–2572.
- [76] TELESCOPE ARRAY collaboration, D. Bergman, *Telescope Array Combined Fit to Cosmic Ray Spectrum and Composition*, *PoS ICRC2021* (2021) 338.
- [77] M. Y. Kuznetsov, N. A. Petrov and Y. S. Savchenko, *Ultra-high energy event KM3-230213A as a cosmogenic neutrino in light of minimal UHECR flux models*, [2509.09590](#).
- [78] M. Kachelriess, O. E. Kalashev and M. Y. Kuznetsov, *Heavy decaying dark matter and IceCube high energy neutrinos*, *Phys. Rev. D* **98** (2018) 083016, [[1805.04500](#)].
- [79] TELESCOPE ARRAY collaboration, J. Kim et al., *Highlights from the Telescope Array Experiment*, *PoS ICRC2023* (2024) 008.
- [80] T. Teshima, Y. Matsubara, T. Hara, N. Hayashida, M. Honda, F. Ishikawa et al., *Properties of 109-1010 gev extensive air showers at core distances between 100 and 3000 m*, *Journal of Physics G: Nuclear Physics* **12** (1986) 1097.
- [81] T. Abu-Zayyad, R. Aida, M. Allen, R. Anderson, R. Azuma, E. Barcikowski et al., *The cosmic-ray energy spectrum observed with the surface detector of the telescope array experiment*, *The Astrophysical Journal Letters* **768** (2013) L1.
- [82] J. Abraham, P. Abreu, M. Aglietta, C. Aguirre, D. Allard, I. Allekotte et al., *Upper limit on the diffuse flux of ultrahigh energy tau neutrinos from the pierre auger observatory*, *Physical Review Letters* **100** (2008) 211101.
- [83] R. Abbasi, M. Abe, T. Abu-Zayyad, M. Allen, R. Azuma, E. Barcikowski et al., *Mass composition of ultrahigh-energy cosmic rays with the telescope array surface detector data*, *Physical Review D* **99** (2019) 022002.